An explicit dynamics framework suited to highly non-smooth interface behaviors

David Dureisseix, Paul Larousse, Anthony Gravouil, Jean Di Stasio

An explicit dynamics framework suited to highly non-smooth interface behaviors

David Dureisseix[1], Paul Larousse[1,2], Anthony Gravouil[1], and Jean Di Stasio[2]

[1] Univ Lyon, INSA Lyon, CNRS, LaMCoS, UMR5259, F-69621 Villeurbanne, France
[2] Centre de technologie de Ladoux, Manufacture française de pneumatiques Michelin, F-63000 Clermont-Ferrand, France

Dynamic systems, and in particular mechanical structures, may be subjected to non-smooth loadings such as impacts or shocks. Moreover, their behavior may itself exhibit more or less non-smooth behaviors, as when fracture occurs. Therefore, robust simulation models are of interest to capture such behaviors. A particular focus is made herein on explicit dynamics schemes to allow efficient simulations, and non-smoothness is embedded within the discrete resolution model, so that robust simulations can be obtained, with a minimal number of numerical parameters. The applications concern non-smooth interface behaviors, are illustrated on simple test cases, and feasibility is shown on a full 3D finite element model.

Keywords matrix-free, perfect plasticity, brittle fracture, finite elements, symplectic scheme, non-locality

1 Non-smoothness is difficult

Non-smooth behaviors in mechanical models often lead to difficulties for their numerical simulation, where the problem is often qualified as stiff. For instance, contact or impact problems, crack propagation, brittle behaviors... involve such difficulties (Brogliato et al. 2002; Acary et al. 2018).

A quasi-static model in this case is usually difficult to tackle, while the use of dynamical behavior may induce some regularization, though rigid models persist in exhibiting several solutions (Moreau 2004; Moreau 2006; Alart 2014). In such cases, but for deformable models, explicit dynamics schemes are useful to reduce the computational cost. Nevertheless, additional regularizations such as penalization are then not suited, since explicit schemes usually exhibit a critical time step that is driven to a possible very small value with high penalization factors in the model.

In this study the focus is therefore on the use of a symplectic explicit scheme, namely the CD-Lagrange scheme (Fekak et al. 2017), embedding by construction the treatment of non-smooth evolutions, without need for any penalization with artificial numerical parameters.

Though non-smooth behaviors may also arise in the bulk of the structure, many different cases often arise also in the contact of an interface (assembling between mechanical parts, heterogeneous structure made with gluing of different parts, interaction between mechanical systems...) Therefore this article focuses on these kinds of non-smooth behaviors. These stiff problems usually require particular formulations to overcome their resolution issue (Jean et al. 2001; de Saxcé 2022).

The CD-Lagrange scheme embedding the non-smooth Moreau framework (Moreau 1986; Moreau 2011; Dubois et al. 2018) involves an interface behavior expressed not with a classical stress vs displacement jump function, but with an impulse-velocity jump relationship. It has been tested and used for different cases of non-regularized frictional contact (Fekak et al. 2017; Di Stasio et al. 2019). It is noteworthy that the different following cases do have some similarities with the non-smoothness involved in the frictional contact models: the rigid, perfect plastic behavior leads to a normal behavior looking similar to the tangential friction of Tresca model; then, the brittle fracture leads to a generalization of the perfect normal contact behavior, the so-called Hertz-Signorini-Moreau (HSM) or Karush-Kuhn-Tucker (KKT) conditions (Wriggers et al. 2007). These cases will be described, implemented and tested in this article.

The target cases considered herein deal with a constant time step Δt, and the small displacement assumption. Moreover, compatible spatial discretizations on each side of an interface are assumed for sake of simplicity; this issue can be overcome for instance by considering the mortar approach (Ben Belgacem et al. 1998; Casadei et al. 2002; Wohlmuth 2000; Popp et al. 2014; Pinto Carvalho et al. 2022).

2 A rigid, perfectly plastic interface behavior

Usually, the perfectly plastic behavior in the bulk of the material may be difficult to tackle in standard finite-element codes. Indeed, the plastic threshold may lead algorithms to fail to converge, especially when non-admissible intermediate solutions are seek for during iterations (Meyer et al. 2022).

Such a behavior may also be considered for normal velocity jump at interface models. Moreover, for an interface, an initial infinite stiffness may also be considered. In such a case, resolution is even more difficult to perform, even in dynamics evolution. Some regularization may be used. For instance a penalized finite stiffness is a classical way to proceed. But the higher the artificial stiffness is (to mimic the infinite asymptotic case), the stiffer the problem is. When one is concerned with explicit dynamics schemes, this cannot be a solution due to the classical conditional stability issue, apart for the fact that the problem itself becomes ill-conditioned. Therefore the rigid case should be taken into account as a non-smooth behavior in the algorithm design.

2.1 Unilateral contact CD-Lagrange scheme

In this section, the classical contact case is recalled to emphasize the different design stages of the algorithm.

For linear dynamics, a spatially discretized (by finite elements) system of mass and stiffness matrices M and K, submitted to an external force is driven by the second-order in time ordinary differential equation (ODE) of the form $M\ddot{U} + KU = f_{\text{ext}}$, where $U(t)$ is the displacement degrees-of-freedom vector and $f_{\text{ext}}(t)$ the external generalized nodal force vector. The CD-Lagrange scheme is based on the central difference time integration scheme, using a desynchronized time discretization where the indices n and $n+1/2$ are related to the time steps t_n and $t_{n+1/2}$. Moreover, as a time-variational scheme, the order of the ODE is reduced by an order 1, and the time-discretized dynamic problem is

$$M(V_{n+3/2} - V_{n+1/2}) + hKU_{n+1} = hf_{\text{ext},n+1} \tag{1}$$

where h is the time step ($h = \Delta t$ assumed herein uniform), and V is the velocity vector, such that $U_{n+1} = U_n + hV_{n+1/2}$ is the explicit computation of the incremental displacement, provided that both U_n and $V_{n+1/2}$ are known, and that U_{n+1} and $V_{n+3/2}$ are seek for.

Moreover, to get an explicit and matrix-free resolution, a classical solution is to use the lumped mass matrix, so M is diagonal, as considered herein. If part of the degrees of freedom (dof) are subjected to unilateral contact condition (without friction in a first step), one may use the localization matrix L containing the dofs selection and projection onto the normal to the contact (which is constant for the small perturbation case studied herein). Therefore, the normal velocity jump at contact interface is $v = LV$, and the normal gap is $g = g_0 + LU$ where g_0 is the initial gap. For impact problems, and moreover for spatially discretized ones, the velocity may exhibit jumps in time, and the acceleration, as well as the contact force are not always defined. The reduced-order system is therefore suited for such a situation, once one introduces the so-called impact impulse r that replaces the contact force and is a convergent quantity when the time step is refined. The discretized non-smooth dynamics evolution equation is then written as

$$M(V_{n+3/2} - V_{n+1/2}) + hKU_{n+1} = hf_{\text{ext},n+1} + L^T r_{n+3/2} \tag{2}$$

or

$$V_{n+3/2} = V_{\text{free}} + M^{-1}L^T r_{n+3/2} \tag{3}$$

where $V_{\text{free}} = V_{n+1/2} + M^{-1}h(f_{\text{ext},n+1} - KU_{n+1})$ would be the velocity if no contact occurs, i.e. if $r_{n+3/2} = 0$.

The reduced dynamics problem consists in expressing from (3) the relation between local unknown quantities at the contact interface $v_{n+3/2}$ and $r_{n+3/2}$. This is done by pre-multiplying with L to get

$$v_{n+3/2} = v_{\text{free}} + Hr_{n+3/2} \tag{4}$$

where $v_{\text{free}} = LV_{\text{free}}$ and $H = LM^{-1}L^T$ is the so-called Delassus operator. When considering compatible finite element meshes between impacting bodies, or impact with a fixed rigid part, the operator L is local to each impacting nodes. Due to the properties of the lumped mass matrix M; this leads to a Delassus operator which is diagonal, definite positive and spherical per node (spatial directions are equivalent, as in the mass matrix M for volumic finite elements) as considered herein.

To close the problem, the local contact behavior should be added, as a relation between impulse and velocity jump. At a potential impacting node, the KKT condition between contact force and displacement jump is replaced, thanks to Moreau viability lemma (Moreau 1999; Dubois et al. 2018), with a relation that can be interpreted as a constitutive relation $\mathcal{R}(v, r; g) = 0$. This relation is nevertheless not smooth nor univoque. It reads:

$$\text{If } g > 0 \text{ then: } r = 0 \tag{5}$$

$$\text{Else: } 0 \leq v \perp r \geq 0 \tag{6}$$

Finally the problem is (4) together with the behavior $\mathcal{R}(v_{n+3/2}, r_{n+3/2}; g_{n+1}) = 0$ and with diagonal Delassus operator, it provides an explicit solution as well. Once $r_{n+3/2}$ is known, the dynamics (3) allows to get the full velocity vector $V_{n+3/2}$.

The classical Coulomb friction laws can also be taken easily into account (Fekak et al. 2017; Di Stasio et al. 2019). Indeed, there are other explicit formulations for contact problems, as the Nitsche approach in (Chouly et al. 2018) but dedicated to deformable bodies.

2.2 A simple oD test case for normal rigid, perfectly plastic behavior

In this new test case, which is expected to be at least as non-smooth as the previous contact case, the only difference resides in the interface behavior, that should be expressed also as an impulse-velocity jump relationship.

The classical representation of the interface behavior, in the normal direction to the interface, is selected to be the parallel association of a perfect contact behavior (with index c) and a purely plastic behavior (with index p) with the stress threshold σ_Y, as depicted on Figure 1. This association leads to the following dual assembly relationships: $r = r_c + r_p$ for the impulses and $v_c = v_p = v$ for the velocity jump (the gap is also the same for both).

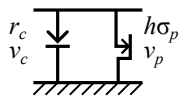

Figure 1: Sketch of the phenomenological interface behavior

The classical plastic behavior part is illustrated on Figure 2. For the perfect plastic behavior, the stress vs displacement jump can be restated as a relationship between impulse and velocity jump v_p as depicted on Figure 3, where we denote $r_Y = h\sigma_Y$, as in all of the following.

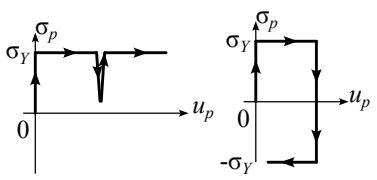

Figure 2: The considered constitutive behavior, as a stress/displacement jump relationship

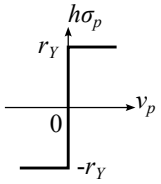

Figure 3: The considered constitutive behavior, as an impulse/velocity jump relationship

When the gap is strictly positive, the contact is disabled, so $r_c = 0$, $r = r_p$, and the reduced dynamics reads

$$v = v_{\text{free}} + Hr_p \tag{7}$$

where $r_p = -h\sigma_p$ (the impulse corresponding to the normal plastic stress, this last one being positive in traction along the normal direction). With the diagonal and positive properties of H, the solution to the intersection of the linear reduced dynamics and non-smooth behavior relations is also explicit as illustrated on Figure 4 and detailed in Algorithm 1.

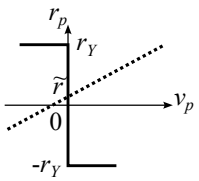

Figure 4: The solution as the intersection of the behavior (plain line) and the reduced dynamics (dotted line)

When the gap is not strictly positive, both the contact and the plastic behaviors are activated. This situation corresponds to the case of an hyperstatic association of two relationships, therefore leading not to a unique solution for each. Nevertheless, the solution is still unique for the sum of the impulses $r = r_c + r_p$ with the reduced dynamics

$$v = v_{\text{free}} + Hr \tag{8}$$

Indeed, consider the cases separation:

- if $v > 0$, then $r_c = 0$, so $r = r_p = -r_Y$ is computed as before. One therefore gets $v = v_{\text{free}} - Hr_Y := \tilde{v}$ that should be positive in this case;
- in the counter case, $v = 0$, and the reduced dynamics reads $0 = v_{\text{free}} + Hr = (v_{\text{free}} - Hr_Y) + H(r_c + r_p + r_Y)$, so $0 = \tilde{v} + H(r_c + r_Y - h\sigma_p)$ for which we should have $r_c \geq 0$ and $0 \leq r_Y - h\sigma_p \leq 2r_Y$. Now if $\tilde{v} > 0$ this is inconsistent and corresponds to the previous case. Therefore $\tilde{v} \leq 0$ and $r = r_c - h\sigma_p = -H^{-1}v_{\text{free}} := \tilde{r}$

This cases separation can therefore be summarized as

- if $\tilde{v} > 0$ (which is equivalent to $\tilde{r} < -r_Y$), then $r = -r_Y$
- else $r = \tilde{r}$

This can be simplified also, as detailed in Algorithm 1.

To illustrate this resolution algorithm, a test case with a single dof problem is considered on Figure 5, with the non-dimensional parameters: $g_0 = 0$, $m = k = 2\sigma_Y = 1$ (the dimensional m would be a mass per unit surface, the dimensional k a stiffness homogeneous to a Young modulus). The characteristic time for the oscillations in the linear regime is $\tau = 2\pi\sqrt{k/m} = 2\pi$. Note that with a single degree-of-freedom problem, the distinction between implicit and explicit scheme is not significant, so there is not a real critical time step in this case and $h = \Delta t$ should be smaller than τ for accuracy criteria; here $h = 0.03$ is chosen.

The results are depicted on Figure 6. The loading consists in successive 3 forth and back increasing tractions followed by a highly dynamic compression whose maximal compression is maintained constant afterwards. The first traction is not high enough to produce plasticity, which can be seen on the displacement evolution: the interface remains perfectly glued. The second traction produces a plastic evolution: the interface plastically separates, and the interface impulse

Input: displacement U_n, velocity $V_{n+1/2}$
Output: displacement U_{n+1}, velocity $V_{n+3/2}$
Displacement $U_{n+1} \leftarrow U_n + hV_{n+1/2}$ ▷ Explicit configuration
$g_{n+1} \leftarrow g_0 + LU_{n+1}$
$V_{\text{free}} \leftarrow V_{n+1/2} + M^{-1}h(f_{\text{ext},n+1} - KU_{n+1})$ ▷ Free velocity
$v_{\text{free}} \leftarrow LV_{\text{free}}$
$\tilde{r} \leftarrow -H^{-1}v_{\text{free}}$
$r_Y \leftarrow h\sigma_Y$
if $g_{n+1} > 0$ **then**
    if $\tilde{r} < -r_Y$ **then** $r_{n+3/2} \leftarrow -r_Y$
    else if $\tilde{r} > r_Y$ **then** $r_{n+3/2} \leftarrow r_Y$
    else $r_{n+3/2} \leftarrow \tilde{r}$
    end if
else $r_{n+3/2} \leftarrow \max(\tilde{r}, -r_Y)$
end if
Velocity $V_{n+3/2} \leftarrow V_{\text{free}} + M^{-1}L^T r_{n+3/2}$ ▷ Matrix-free dynamics

Algorithm 1: Time step increment for the perfect plastic interface

is constant during perfect plasticity. Finally the plasticity develops even more during the third traction, while the brutal compression allows to plastify in compression, up to the perfect contact activation with a velocity jump and an impact impulse.

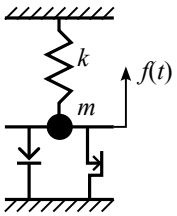

Figure 5: Sketch of the test case

3 A rigid, brittle interface with adhesion recovery

An even more non-smooth case is designed herein for testing purpose as an interface behavior that could be called "non-smooth post-it™".

As for the previous example, a 0D test (i.e. in normal direction of the interface only) is first considered, and will after be generalized to a 2D interface.

Though fracture models are usually derived from energy release when creating fracture surface (Francfort 2006; Kiener et al. 2022), the brittle fracture is usually associated to a small energy. The contact part of the interface behavior is one source of non-smoothness (Jean et al. 2001). The infinite stiffness in traction of the interface (before fracture) is a second one (Collins-Craft et al. 2022). Finally the limit case of perfectly brittle fracture, which is tested herein, exhibits a higher non-smooth response, corresponding to null energy dissipation. Though the physical interpretation of this limit case is not trivial (usually, looking at a physical smaller scale leads to some elastic behavior and some dissipation, Raffa et al. 2022; Lebon et al. 2022), this case is used herein to challenge the models, leading to difficult numerical non-smoothness issues. Indeed this limit case is not well posed for quasi-static problems, since it would lead to an instability leading to instantaneous debonding of interfaces.

3.1 A normal behavior test with a 0D problem

The considered constitutive behavior is a compound of two different situations: a perfect contact or a gluing behavior with a yield traction load f_Y (or impulse $r_Y = hf_Y$) above which a brittle rupture occurs. The sketch of this behavior is depicted in Figure 7. In compression, the unilateral contact prevents the interpenetration.

The reduced dynamics reads $v = v_{\text{free}} + Hr$. As before, with the diagonal and positivity

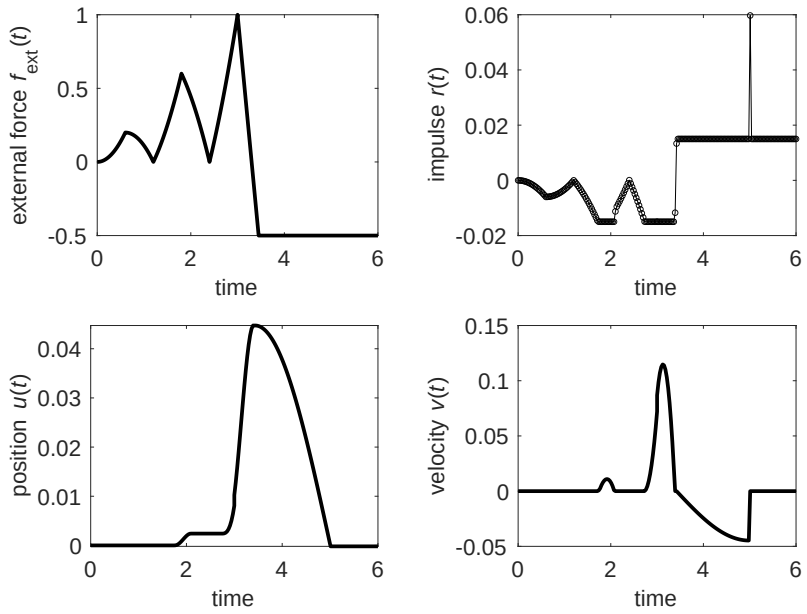

Figure 6: The numerical solution for the oD test case for the perfectly plastic interface

properties of H, the solution is the intersection of the behavior and the reduced dynamics as illustrated on Figure 8, when the gap is null.

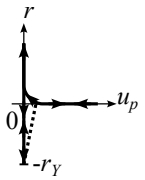

Figure 7: The considered brittle constitutive behavior, as an impulse/displacement jump relationship (the dotted line denotes a brutal jump in the status)

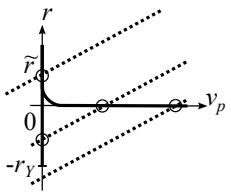

Figure 8: The brittle fracture solution as the intersection of the impulse/velocity behavior (plain line) and the reduced dynamics (dotted line)

When the gap is strictly positive, the fracture has occurred, so $r = 0$.

When the gap is not strictly positive, three different cases may happen:

- either $\tilde{r} \leq -r_Y$, then the solution is $r = 0$ (and $v \geq 0$, the fracture occurs);
- or $\tilde{r} > 0$, then the solution is $r = \tilde{r}$ (and $v = 0$, the contact is active);
- else, there are two possible solutions. In this case, the continuity of the previous status allows to decide which one is selected: either the previous status was inactive contact, so the status does not evolve and $r = 0$, or the previous status was active contact or glued, and the status is now glued and $r = \tilde{r}$.

This behavior does nevertheless not take into account that the yield stress f_Y may evolve (and is therefore an internal variable). Indeed, the considered modified model is: when a rupture occurs, f_Y is nullified; when the impulse is positive (compression), f_Y may increase back (this is a recovery of adhesion). An induced simplification also resides in the previous status of the interface: it has been stored in the f_Y internal variable, so that the $f_Y = 0$ case corresponds to the case where a fracture has occurred, and the constitutive behavior then collapses into the classical unilateral contact behavior; this allows to a more compact sub-cases selection (only two

remaining): indeed, if rupture has occurred, one has $f_Y = r_Y = 0$, so that the first two previous cases cover all the possibilities.

An issue concerns the choice of the variable representing the threshold that should be a material intrinsic parameter. It was previously mentioned that either a yield stress f_Y or an impulse distribution r_Y are used, related with $r_Y = hf_Y$. Therefore, h being a discretization parameter, f_Y and r_Y cannot both be intrinsic material parameters. An answer could a priori be obtained by looking at convergence of the solution when the time step h goes to zero. If a oD problem is considered, loaded with an external force $f_{\text{ext}}(t)$, and a material parameter r_Y, the impulse solution looks like $r(t) = -hf_{\text{ext}}(t)$, therefore r tends toward o (and r/h has a finite limit), so whatever the load is, after a certain refinement in time discretization, one cannot have $r \leq -r_Y$, so there is an inconsistency. Now consider a oD problem, loaded with an external impulse $r_{\text{ext}}(t)$ (so that the equivalent force is $f(t) = r_{\text{ext}}(t)/h$). If the material parameter is f_Y, since the solution looks like $r(t) = r_{\text{ext}}(t)$, after a certain refinement, and whatever the load is, one will always have $r > -r_Y = hf_Y$, so there is also an inconsistency.

Two physical fracture modes may be considered, that are physically different: either due to a smooth force, or due to a shock, so that the failure criteria is a compound: $r < -r_Y$ *or* $r < -hf_Y$. Herein, another physical model is considered: though the fracture happens brutally in time, the quantity that drives the fracture mechanism could be non-local in time. Indeed, at each interface point the quantity $R(t) = \int_{t-\tau_Y}^{t} f(t)dt$ may be defined, where f is the interface normal stress, which is equivalent to the more general expression $R(t) = \sum_{i,t_i \in [t-\tau_Y,t]} r(t_i)$ homogeneous to an impulse. Its interpretation is that a smooth force may lead to a brittle fracture, provided that is has been applied during a sufficient time duration, and that shocks may also lead to a brittle fracture, provided that they have been repeated sufficiently rapidly or have been sufficiently intense. With this new quantity, the fracture criteria reads $R < -R_Y$, where R_Y is a material parameter homogeneous to an impulse distribution, together with a second intrinsic parameter, namely a characteristic time τ_Y. As mentioned previously, one may consider a variable-in-time R_Y. R_Y is nullified when fracture occurs, and can be recovered by normal compression, i.e. when $r > 0$. A consistent criteria could then read: $R_Y(t) = \max(R_Y(t); R(t))$. And finally a maximum recovery could be added with a third material parameter, $R_{Y\max}$ leading to $R_Y(t) = \min(R_{Y\max}; \max(R_Y(t); R(t)))$. Such a modification with a non-locality in time is not related to a smoothing since no modification is made on the instantaneous fracture event, contrary to smoothing evolutions as in (Zhang et al. 2019).

A main implementation difference is due to the non-locality in time: the impulse field r should be stored during a previous duration of τ_Y, as a moving window in time. This indeed leads to a higher storage cost, but does not prevent the explicit matrix-free feature of the algorithm.

A bit more general model can be selected, such as one with an efficiency decrease of the adhesion recovery. Another internal variable is then used: α, that measures the efficiency of the adhesion recovery: as an initial condition, $\alpha = 1$ (maximum efficiency). At each fracture event at time t, it is then decreased, for instance with the following evolution law: $\alpha(t^+) = \alpha(t^-)e^{-1/n_b}$, where n_b is then an additional material parameter. This is a discrete evolution: the decrease of efficiency is not continuous in time, but occurs at fracture events. The Algorithm 2 implements the non-locality in time and the possible decrease in adhesion recovery efficiency.

It can also be noticed that when this non-smooth brittle fracture occurs, no energy is dissipated in the interface ($r = 0$, so $v^T r = 0$), this could therefore be called a perfectly brittle behavior.

The following test case is implemented: consider again the mechanical system of Figure 5, still with a dimensionless mass $m = 1$, but without stiffness $k = 0$ and with a brittle interface behavior. As a load, some shocks are produced, i.e. an external impulse $r_{\text{ext}}(t)$ is prescribed, Figure 9. Concerning the time discretization, 160 time steps of uniform duration h are selected. The initial conditions (null displacement, negative initial velocity) are designed so that a periodic solution is obtained for the first following test.

Several tests are proposed:

- The test 1 consists of using as material parameters $R_{Y\max} = \infty$ (no adhesion limit), $n_b = \infty$ (no efficiency decrease), $\tau_Y = 0$ (no delay effect). For these values, a cyclic response is

Input: U_n and $V_{n+1/2}$ as well as interface status $R_{Y,n+1/2}$ and $\alpha_{n+1/2}$
Output: U_{n+1} and $V_{n+3/2}$ as well as new interface status $R_{Y,n+3/2}$ and $\alpha_{n+3/2}$

Displacement $U_{n+1} \leftarrow U_n + hV_{n+1/2}$ ▷ Explicit configuration
$g_{n+1} \leftarrow g_0 + LU_{n+1}$
$V_{\text{free}} \leftarrow V_{n+1/2} + M^{-1}h(f_{\text{ext},n+1} - KU_{n+1})$ ▷ Free velocity
$v_{\text{free}} \leftarrow LV_{\text{free}}$
if $g_{n+1} > 0$ **then** ▷ Inactive interaction
  $\alpha_{n+3/2} \leftarrow \alpha_{n+1/2}$
  $R_{Y,n+3/2} \leftarrow 0$
  $r_{n+3/2} \leftarrow 0$
else
  $\tilde{r} \leftarrow -H^{-1}v_{\text{free}}$
  $\tilde{R} \leftarrow \tilde{r} + \sum_{i,t_i \in [t_{n+3/2}-\tau_Y, t_{n+1/2}]} r_i$
  $\tilde{R}_Y \leftarrow \min(R_{Y\max}; \max(R_{Y,n+1/2}; \alpha_{n+1/2}\tilde{R}))$
  if $\tilde{R} > -\tilde{R}_Y$ **then** ▷ Glued interaction
    $\alpha_{n+3/2} \leftarrow \alpha_{n+1/2}$
    $R_{Y,n+3/2} \leftarrow \tilde{R}_Y$
    $r_{n+3/2} \leftarrow \tilde{r}$
  else
    if $\tilde{R}_Y > 0$ **then** ▷ Brittle fracture occurs
      $\alpha_{n+3/2} \leftarrow \alpha_{n+1/2}e^{-1/n_b}$ ▷ Adhesion efficiency decrease
    else
      $\alpha_{n+3/2} \leftarrow \alpha_{n+1/2}$
    end if
    $R_{Y,n+3/2} \leftarrow 0$
    $r_{n+3/2} \leftarrow\!< \tilde{r} >_+$
  end if
end if
Velocity $V_{n+3/2} \leftarrow V_{\text{free}} + M^{-1}L^T r_{n+3/2}$ ▷ Matrix-free dynamics

Algorithm 2: Time step increment for the brittle fracture interface (normal behavior only)

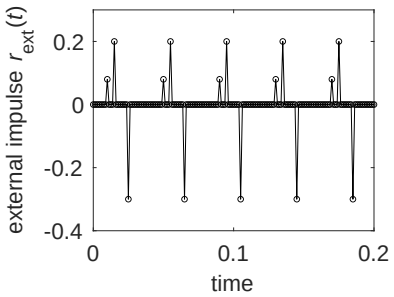

Figure 9: The non-smooth loading for the 0D test cases

test	1	2	3	3D
efficiency decrease n_b	∞	10	∞	∞
adhesion limit $R_{Y\max}$	∞	∞	∞	10^{-4}
delay effect τ_Y	0	0	0.08	0.2
normal to tangent influence λ	-	-	-	0.8
friction coefficient μ	-	-	-	0.1

Table 1: Interface non-dimensional parameters for the different test cases

produced, Figure 10. A first impulse $r(t = h) > 0$ is produced due to the initial condition that engenders a compressive shock and increases the yield impulse R_Y; then a negative impulse happens opposed to the external first positive shock r_{ext} which is not large enough to produce a fracture; the second external impulse is large enough for a fracture to happen (the impulse r is therefore null, as the yield impulse R_Y), and to induce kinetic energy of detachment. The third external impulse in negative and has been adjusted to get back the mass into contact with a positive impulse r identical to the initial one, so cycling is obtained afterwards. Thanks to good discrete energy conservation of the integration scheme, cycles are preserved at long time duration.

- For the test 2, only the efficiency decrease is changed to $n_b = 10$. The solution is no more cyclic, Figure 11. Indeed the yield impulse reconstruction R_Y decreases up to the point when the first type of external impulse can produce the fracture, so the impulse and velocity solutions are no more cyclic.
- The test 3 uses the same parameters as for test 1, except that a delay effect is used with $\tau_Y = 0.08$ (actually 64 time steps). Though the solution differs from test 1 for the yield R_Y, Figure 12, due to the time delay that is a moving window in time, the associated material behavior is conservative, are allows to recover the same solution for the other quantities.

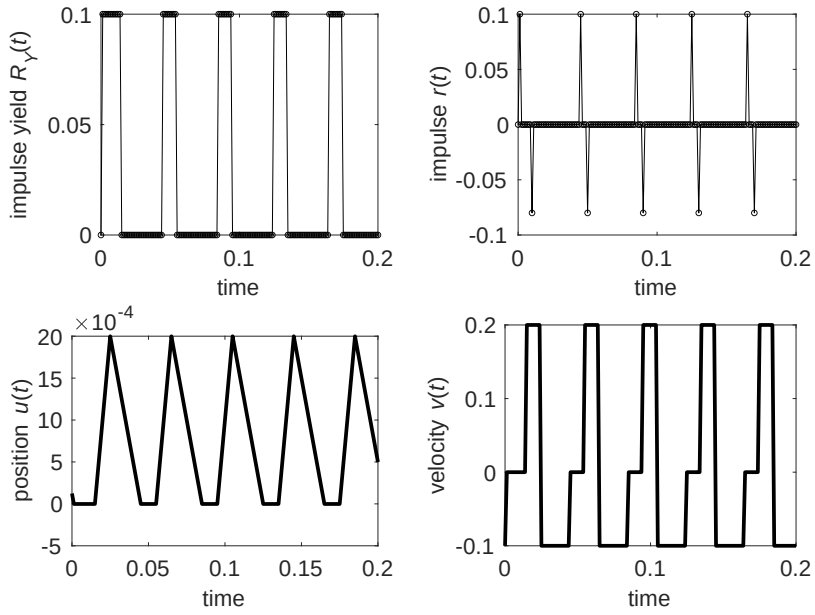

Figure 10: The numerical solution for the first oD brittle test case

To check time-convergence, an additional test is used, based on the previous test 3, but with an additional smooth loading $f_{\text{ext}}(t) = -F_d \sin(\frac{4}{5}\pi t/T_c)$ with a non-dimensional amplitude $F_d = 2$, $T_c = 0.04$ being the non-dimensional duration of one cycle. Different time steps are used, and an over-killing one is used to obtain a reference solution ($h_{\text{ref}} \approx 7.63\ 10^{-8}$). Since for instance the velocity is discontinuous, a Hausdorff distance (Moreau 1978; Acary 2012) is used to get an error with respect to this reference, both for the displacement and the velocity solutions. Note that normalizations of evolution graphs are needed for the metric of such a norm: the time scale is rescaled as t/T, T being the total studied time duration and both displacement and velocity are rescaled with respect to their maximum absolute values of the reference solutions. In such a way the Hausdorff distance is an absolute error measure and is reported on Figure 13.

Apart from checking the convergence, and as expected for this central-difference-like scheme for non-smooth problems, a convergence rate of $O(h)$ is obtained, see e.g. (Chen et al. 2013).

3.2 3D structures and surfacic interfaces

To start with, the interface behavior is considered with a normal f_N and a tangential force distribution (or stress) $\underline{f}_T$, together with a yield stress σ_Y at an interface point. No non-locality in time are considered in a first step.

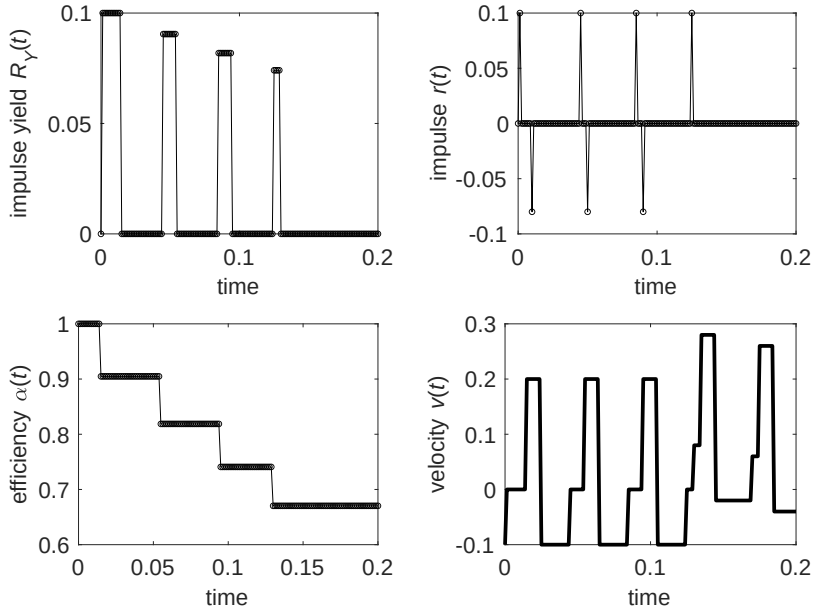

Figure 11: The numerical solution for the second oD brittle test case

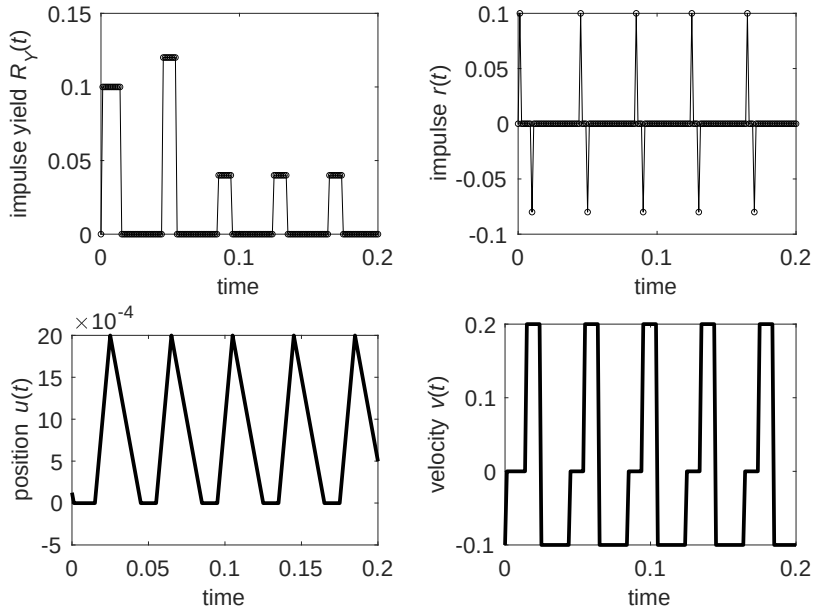

Figure 12: The numerical solution for the third oD brittle test case

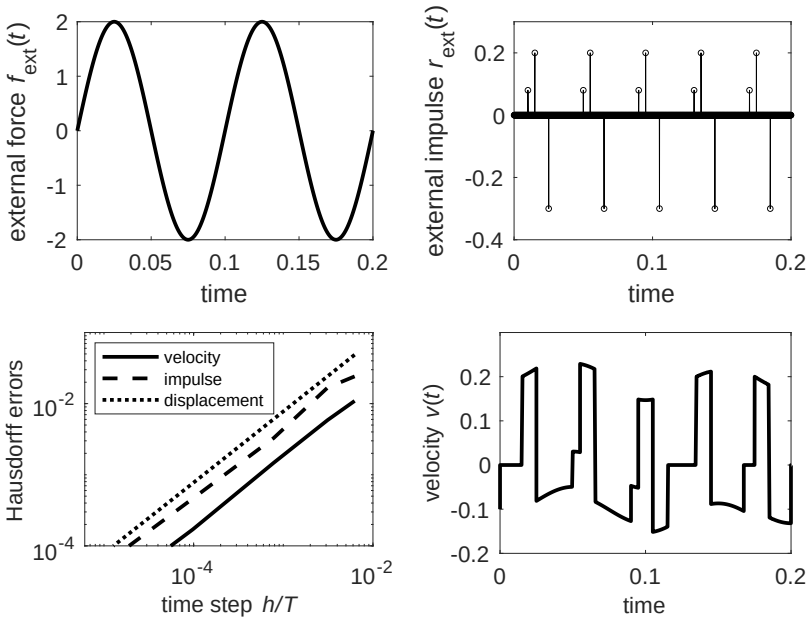

Figure 13: The loading with forces and impulses, the numerical convergence of the solution with respect to time discretization and the reference solution for velocity

Since fracture may happen with a shear stress, a threshold criteria should be used. A proposed equivalent stress is defined as

$$\sigma(f_N, \underline{f}_T) = \sqrt{< f_N >_+^2 + \|\underline{f}_T\|^2/\lambda^2} \tag{9}$$

so only the tension normal part (hence the positive part $< f_N >_+$ is involved) acts on the fracture, and where λ is a weight for the influence of the tangential part, Figure 14. When $\sigma(f_N, \underline{f}_T) < \sigma_Y$ no fracture occurs and the interface status is 'glued', i.e. the velocity jump is $\underline{v} = 0$; when $\sigma(f_N, \underline{f}_T) > \sigma_Y$ a fracture has occurred and the interface status is 'contact', i.e. unilateral contact with Coulomb tangential friction, with a friction coefficient μ, that may be either inactive ($v_N > 0$, $f_N = 0$, $\underline{f}_T = 0$) or sliding ($\underline{v}_T \neq 0$, $f_N > 0$, $\|\underline{f}_T\| = \mu f_N$) or sticking ($\underline{v}_T = 0$, $f_N > 0$, $\|\underline{f}_T\| \leq \mu f_N$). In this considered model, no smooth transition occurs between the glued and contact status, to keep the behavior as non smooth as possible for testing the proposed resolution algorithms.

It can be noticed that when $\sigma_Y = 0$, the threshold collapses to the positive semi-axis $f_N < 0$. When $\lambda = \infty$ the tangential direction has no influence on the fracture, the normal behavior is identical as in the 0D test case. When $R_{Y\max} = 0$, the behavior reduces to a classical contact with Coulomb friction.

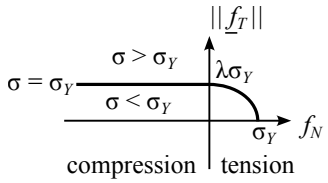

Figure 14: Yield function for 2D fracture criteria

Since with a 2D interface, tangential components are involved as vector quantities, underlying has been used to differentiate them from scalar quantities. Note however that in the following, when dealing with discretized quantities as column vectors, no underlying will be used anymore.

The resolution algorithm 3 is then built on the same framework as previously. In particular, the velocity-impulse formulation is used, with $r_Y = h\sigma_Y$, $r_N = -hf_N$, $r_T = -hf_T$, but as 3D cases discretized by finite elements are concerned, one has to add a loop on the nodes of the interface. The non-locality in time and the adhesion recovery decrease are also trivially extended to these cases.

Moreover, since the local quantities on the interface are impulse distributions, an additional integration on the interface has to be performed. To keep these quantities at nodal position on the interface, a nodal integration is therefore selected, the integration weight at node k is $S^{(k)}$. To simplify the notations, their assembling on the full set of dofs will be denoted with the diagonal entry matrix S, with duplicated entries on the 3 spatial directions and 3 zeros entries on the nodes that are not located on the interface. For 3D cases, the dynamics therefore reads

$$V_{n+3/2} = V_{\text{free}} + M^{-1}SL^T r_{n+3/2} \tag{10}$$

$$= V_{\text{free}} + M^{-1}SL_N^T r_{N,n+3/2} + M^{-1}SL_T^T r_{T,n+3/2} \tag{11}$$

where the mapping operators L_N^T and L_T^T contain respectively the normal to the interface, two tangent directions at the interface, and the mapping to the global dofs. With the previously mentioned properties of matrix M, still valid in 3D, and similar properties for S, one has $L_N M^{-1} S L_T^T = 0$ so that the reduced dynamics reads firstly: $v_N = v_{N\text{free}} + H_N r_N$, where $H_N = L_N M^{-1} S L_N^T$, $v_{N\text{free}} = L_N V_{\text{free}}$, and secondly: $v_T = v_{T\text{free}} + H_T r_T$, where $H_T = L_T M^{-1} S L_T^T$, $v_{T\text{free}} = L_T V_{\text{free}}$. The Delassus operators H_N and H_T are still definite positive, diagonal and spherical per node entry.

Concerning the energy conservation, no energy is lost during fracture, but kinetic energy of back impacting node is lost at impact (no Newton restitution coefficient is used). This is a drawback of the discretized problem (the energy loss is driven to zero when mesh size is refined), but can be dealt with using an advanced modeling of mass matrix: the so-called redistributed or singular mass technique (Khenous et al. 2008; Tkachuk et al. 2013; Dabaghi et al. 2019; Di Stasio et al. 2021). There is also a physical source of energy loss, due to the friction between fractured surfaces, driven by the friction coefficient μ.

3.3 3D test case

The 3D test case is modeled with classical finite elements, the geometry is given on Figure 15. It consists on a one-fourth of a tube slice (the internal radius is $R_1 = 1$, the thickness $L_1 = 0.5$ and the length $L_2 = 0.5$). meshed with 5712 cubic elements with 4 nodes each, leading to 20475 dof. The non-dimensional volumic parameters are: a Young modulus $E = 1$, a Poisson coefficient $\nu = 0.3$ and a density of $\rho = 1$. Two interfaces with the rigid foundation are considered, on the two rectangular ends of the tube quarter. Both have the same behavior, whose parameters are given in Table 1. With the previous spatial discretization, there are 390 interface nodes.

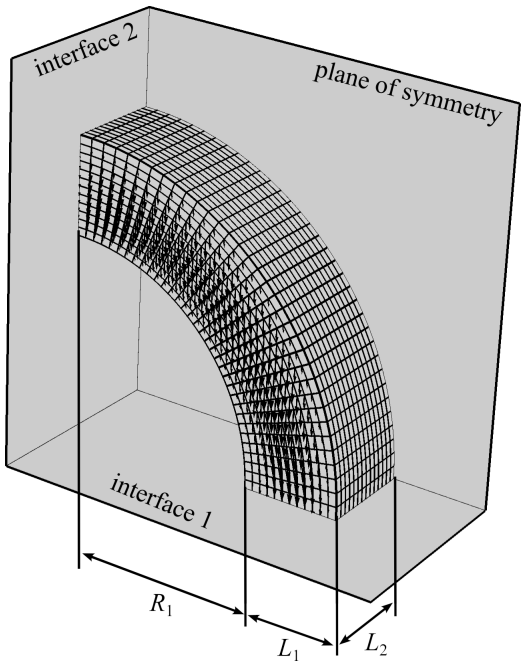

Figure 15: Geometry of the 3D test case, with the vertical shear stress on the face end

The boundary conditions are a symmetry plane, and a shear stress on the other end face (a quadratic radial distribution, whose resultant value is depicted on Figures 16 (a) and (c))

Input: U_n and $V_{n+1/2}$ as well as interface status fields $R_{Y,n+1/2}$ and $\alpha_{n+1/2}$
Output: U_{n+1} and $V_{n+3/2}$ as well as new interface status fields $R_{Y,n+3/2}$ and $\alpha_{n+3/2}$

Displacements $U_{n+1} \leftarrow U_n + hV_{n+1/2}$ ▷ Explicit configuration
$g_{n+1} \leftarrow g_0 + LU_{n+1}$
$V_{\text{free}} \leftarrow V_{n+1/2} + M^{-1}h(f_{\text{ext},n+1} - KU_{n+1})$ ▷ Free velocity
for each interface point k **do**
  $v_{N\text{free}} \leftarrow L_N^{(k)} V_{\text{free}}$ ▷ With the local to node k operator
  $v_{T\text{free}} \leftarrow L_T^{(k)} V_{\text{free}}$
  if $g_{n+1}^k > 0$ **then** ▷ Inactive interaction
    $\alpha_{n+3/2} \leftarrow \alpha_{n+1/2}$
    $R_{Y,n+3/2} \leftarrow 0$
    $r_{N,n+3/2} \leftarrow 0$
    $r_{T,n+3/2} \leftarrow 0$
  else
    $\tilde{r}_N \leftarrow -H_N^{-1} v_{N\text{free}}$
    $\tilde{r}_T \leftarrow -H_T^{-1} v_{T\text{free}}$
    $\tilde{R}_N \leftarrow \tilde{r}_N + \sum_{i,t_i \in [t_{n+3/2}-\tau_Y, t_{n+1/2}]} r_{N,i}$
    $\tilde{R}_T \leftarrow \tilde{r}_T + \sum_{i,t_i \in [t_{n+3/2}-\tau_Y, t_{n+1/2}]} r_{T,i}$
    $\tilde{R}_Y \leftarrow \min(R_{Y\max}; \max(R_{Y,n+1/2}; \alpha_{n+1/2}\tilde{R}_N))$
    if $\sigma(-\tilde{R}_N, -\tilde{R}_T) < \tilde{R}_Y$ **then** ▷ Glued interaction
      $\alpha_{n+3/2} \leftarrow \alpha_{n+1/2}$
      $R_{Y,n+3/2} \leftarrow \tilde{R}_Y$
      $r_{N,n+3/2} \leftarrow \tilde{r}_N$
      $r_{T,n+3/2} \leftarrow \tilde{r}_T$
    else
      if $R_{Y,n+1/2} > 0$ **then** ▷ Brittle fracture occurs
        $\alpha_{n+3/2} \leftarrow \alpha_{n+1/2} e^{-1/n_b}$ ▷ Adhesion efficiency decrease
      else
        $\alpha_{n+3/2} \leftarrow \alpha_{n+1/2}$
      end if
      $R_{Y,n+3/2} \leftarrow 0$
      if $\tilde{r}_N > 0$ **then** ▷ Active contact
        $r_{N,n+3/2} \leftarrow \tilde{r}_N$
        if $\|\tilde{r}_T\| > \mu r_{N,n+3/2}$ **then** ▷ Sliding
          $r_{T,n+3/2} \leftarrow \mu r_{N,n+3/2} \frac{\tilde{r}_T}{\|\tilde{r}_T\|}$
        else ▷ Sticking
          $r_{T,n+3/2} \leftarrow \tilde{r}_T$
        end if
      else ▷ Released contact
        $r_{N,n+3/2} \leftarrow 0$
        $r_{T,n+3/2} \leftarrow 0$
      end if
    end if
  end if
  Assemble $r_{N,n+3/2}$ and $r_{T,n+3/2}$ in the right-hand-side $r_{n+3/2}$
end for
Velocity $V_{n+3/2} \leftarrow V_{\text{free}} + M^{-1}SL^T r_{n+3/2}$ ▷ Matrix-free dynamics

Algorithm 3: Time step increment for the 2D brittle fracture interface

engendering a non-uniform solicitation both with normal and tangential components on the interfaces. Two time evolutions of the loading are considered, Figure 16 (a) and (c), the first one being less smooth than the second and involving more dynamical effects.

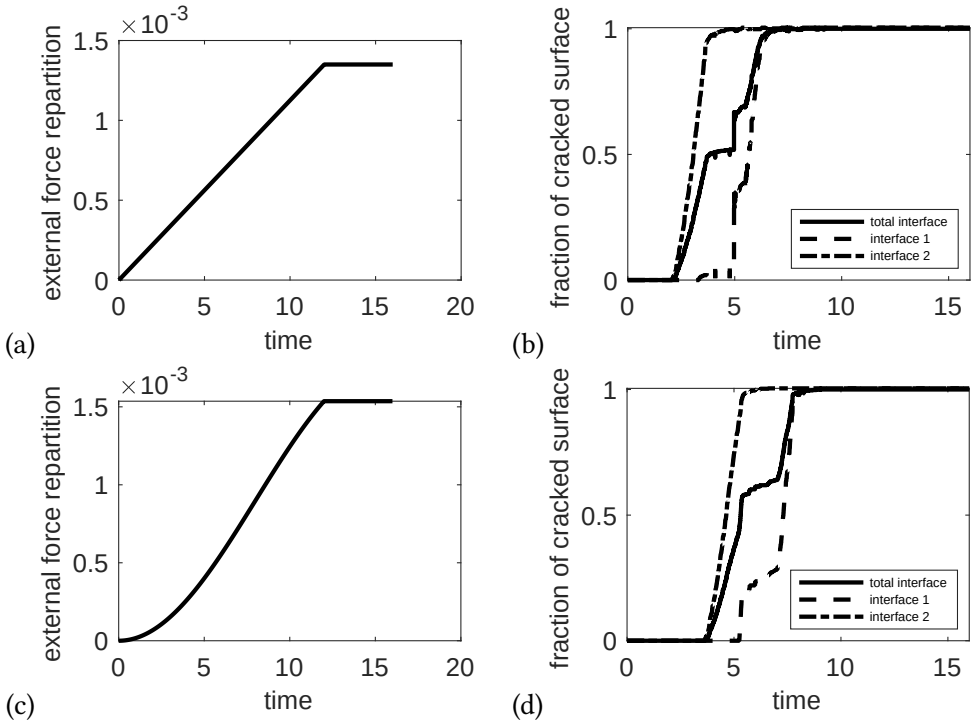

Figure 16: (a) test case 1, and (c) test case 2: time loading evolutions; (b) test case 1, and (d) test case 2: evolutions of the fraction of cracked surfaces

The initial conditions are a null displacement and velocity, and an initial adhesion threshold $R_Y(t=0) = 10^{-4}$. The studied time interval is $T = 16$, with a time step $h = T/8000 = 0.002$, while the estimated critical time step is $t_c \approx 0.047$.

One can note that there could be some unstable initial determination of the evolution of the state variables, subjected to numerical precision issues when one uses at initial condition both an initial gap $g_0 = 0$ and an initial velocity $V_0 = 0$. Indeed, this corresponds to a grazing contact for which the distinction between active and inactive contact is undetermined. To fix this issue, a simple solution is to initialize the initial gap with a 'small' value (larger than the numerical precision), e.g. $g_0 = -10^{-10}$, so that the initial state is active contact.

If $\lambda = \infty$ (no influence of tangential component), no failure occurs for this test case, since the interfaces are subjected to a normal compression. On the other hand, with the selected value of λ of Table 1, shearing is taken into account and the evolution of the fraction of cracked surface of the interfaces are depicted on Figure 16 (b) and (d), for the two loading time evolutions. Indeed, the smooth loading leads to a delayed fracture, since the loading increases slower than for the first case. Moreover, the fracture curves are smoother as well, since there are less forward and backward elastic waves traveling in the structure. In each case, we can observe that the fracture, induced mainly herein by shearing of the interface, is first developing in the interface number 2, Figure 15, more subjected to shearing.

4 Conclusions and perspectives

The previously developed symplectic and explicit dynamic scheme CD-Lagrange has been tested on different highly non-smooth behaviors localized in mechanical interfaces. It provides a framework for the implementation of non-smooth (and not regularized) relationships, provided that the constitutive behaviors are expressed between impulse and velocity. Perfect plasticity with rigid interface and perfectly brittle fracture have been tested for a single degree-of-freedom problem, and validated on a full 3D finite element peeling-like problem.

Non-smooth (and non-univoque) constitutive relations may also lead to the so-called

deterministic chaos, i.e. an a priori deterministic problem that may have a unique solution, but whose solution may strongly depend on initial conditions, so that a small perturbation may engender a different local answer. This issue nevertheless resides in the model, and the explicit algorithm would produce a feasible solution.

Concerning perspectives, some less non-smooth cases can also be studied, as ductile damage (cohesive zone models), for which an extrinsic case is feasible with no initial compliance (Collins-Craft et al. 2022). To avoid spatial localization a delay-effect model (Needleman 1988; Allix et al. 1997; Allix et al. 2003; Desmorat et al. 2010) will be more suited since non-locality in space (Pijaudier-Cabot et al. 1987; Lasry et al. 1988; Kamensky et al. 2022) would prevent an explicit matrix-free approach. Generalization to asynchronous explicit schemes (Gravouil et al. 2014; Niu et al. 2022) is also under concern.

Funding We gratefully acknowledge the French National Association for Research and Technology (ANRT, CIFRE grant number 2021/0957). This work was supported by the "Manufacture Française de Pneumatiques Michelin".

Bibliographic references

Acary, V. (2012). "Higher order event capturing time-stepping schemes for nonsmooth multibody systems with unilateral constraints and impacts". *Applied Numerical Mathematics* 62.10, pp. 1259–1275. DOI: 10.1016/j.apnum.2012.06.026. URL: https://hal.science/inria-00476398/

Acary, V., M. Brémond, and O. Huber (2018). "On solving contact problems with Coulomb friction: Formulations and numerical comparisons". *Advanced Topics in Nonsmooth Dynamics*. Springer International Publishing, pp. 375–457. DOI: 10.1007/978-3-319-75972-2_10. URL: https://hal.science/hal-01878539

Alart, P. (2014). "How to overcome indetermination and interpenetration in granular systems via nonsmooth contact dynamics. An exploratory investigation". *Computer Methods in Applied Mechanics and Engineering* 270, pp. 37–56. DOI: 10.1016/j.cma.2013.11.020. URL: https://hal.science/hal-02075883

Allix, O. and J.-F. Deü (1997). "Delayed-damage modelling for fracture prediction of laminated composites under dynamic loading". *Engineering Transactions* 45.1, pp. 29–46. DOI: 10.24423/engtrans.680.1997. URL: https://et.ippt.gov.pl/index.php/et/article/view/680/501

Allix, O., P. Feissel, and P. Thévenet (2003). "A delay damage mesomodel of laminates under dynamic loading: basic aspects and identification issues". *Computers & Structures* 81.12, pp. 1177–1191. DOI: 10.1016/s0045-7949(03)00035-x

Ben Belgacem, F., P. Hild, and P. Laborde (1998). "The mortar finite element method for contact problems". *Mathematical and Computer Modelling* 28.4-8, pp. 263–271. DOI: 10.1016/s0895-7177(98)00121-6

Brogliato, B., T. ten Dam, L. Paoli, F. Génot, and M. Abadie (2002). "Numerical simulation of finite dimensional multibody nonsmooth mechanical systems". *Applied Mechanics Reviews* 55.2, pp. 107–150. DOI: 10.1115/1.1454112. URL: https://hal.science/hal-01349852/

Casadei, F., E. Gabellini, G. Fotia, F. Maggio, and A. Quarteroni (2002). "A mortar spectral/finite element method for complex 2D and 3D elastodynamic problems". *Computer Methods in Applied Mechanics and Engineering* 191.45, pp. 5119–5148. DOI: 10.1016/s0045-7825(02)00294-3

Chen, Q. Z., V. Acary, G. Virlez, and O. Brüls (2013). "A nonsmooth generalized-α scheme for flexible multibody systems with unilateral constraints". *International Journal for Numerical Methods in Engineering* 96.8, pp. 487–511. DOI: 10.1002/nme.4563. URL: https://hal.science/hal-00858066

Chouly, F. and Y. Renard (2018). "Explicit Verlet time-integration for a Nitsche-based approximation of elastodynamic contact problems". *Advanced Modeling and Simulation in Engineering Science* 5.1, pp. 31–68. DOI: 10.1186/s40323-018-0124-5. URL: https://hal.science/hal-01814774

Collins-Craft, N. A., F. Bourrier, and V. Acary (2022). "On the formulation and implementation of extrinsic cohesive zone models with contact". *Computer Methods in Applied Mechanics and Engineering* 400, p. 115545. DOI: 10.1016/j.cma.2022.115545

Dabaghi, F., P. Krejčí, A. Petrov, J. Pousin, and Y. Renard (2019). "A weighted finite element mass redistribution method for dynamic contact problems". *Journal of Computational and Applied*

Mathematics 345, pp. 338–356. DOI: 10.1016/j.cam.2018.06.030. URL: https://hal.science/hal-01237748

de Saxcé, G. (2022). "A non incremental variational principle for brittle fracture". *International Journal of Solids and Structures* 252, p. 111761. DOI: 10.1016/j.ijsolstr.2022.111761. URL: https://arxiv.org/abs/2112.03065

Desmorat, R., M. Chambart, F. Gatuingt, and D. Guilbaud (2010). "Delay-active damage versus non-local enhancement for anisotropic damage dynamics computations with alternated loading". *Engineering Fracture Mechanics* 77.12, pp. 2294–2315. DOI: 10.1016/j.engfracmech.2010.04.006. URL: https://hal.science/hal-00994292

Di Stasio, J., D. Dureisseix, G. Georges, A. Gravouil, and T. Homolle (2021). "An explicit time-integrator with singular mass for non-smooth dynamics". *Computational Mechanics* 68.1. Ed. by S. Verlag, pp. 97–112. DOI: 10.1007/s00466-021-02021-5. URL: https://hal.science/hal-03212569/

Di Stasio, J., D. Dureisseix, A. Gravouil, G. Georges, and T. Homolle (2019). "Benchmark cases for robust explicit time integrators in non-smooth transient dynamics". *Advanced Modeling and Simulation in Engineering Sciences* 6.1. DOI: 10.1186/s40323-019-0126-y. URL: https://amses-journal.springeropen.com/counter/pdf/10.1186/s40323-019-0126-y

Dubois, F., V. Acary, and M. Jean (2018). "The Contact Dynamics method: A nonsmooth story". *Comptes Rendus Mécanique* 346.3, pp. 247–262. DOI: 10.1016/j.crme.2017.12.009. URL: https://hal.science/hal-01676287

Fekak, F.-E., M. Brun, A. Gravouil, and B. Depale (2017). "A new heterogeneous asynchronous explicit–implicit time integrator for nonsmooth dynamics". *Computational Mechanics* 60.1, pp. 1–21. DOI: 10.1007/s00466-017-1397-0. URL: https://hal.science/hal-01852099

Francfort, G. A. (2006). "Quasistatic brittle fracture seen as an energy minimizing movement". *GAMM-Mitteilungen* 29.2, pp. 172–191. DOI: 10.1002/gamm.201490029

Gravouil, A., A. Combescure, and M. Brun (2014). "Heterogeneous asynchronous time integrators for computational structural dynamics". *International Journal for Numerical Methods in Engineering* 102.3-4, pp. 202–232. DOI: 10.1002/nme.4818

Jean, M., V. Acary, and Y. Monerie (2001). "Non-smooth contact dynamics approach of cohesive materials". *Philosophical Transactions of the Royal Society of London. Series A: Mathematical, Physical and Engineering Sciences* 359.1789. Ed. by F. G. Pfeiffer, pp. 2497–2518. DOI: 10.1098/rsta.2001.0906. URL: https://hal.science/inria-00423556

Kamensky, D., M. D. Alaydin, and Y. Bazilevs (2022). "A Review of Nonlocality in Computational Contact Mechanics". *Current Trends and Open Problems in Computational Mechanics*. Springer International Publishing, pp. 239–246. DOI: 10.1007/978-3-030-87312-7_23

Khenous, H. B., P. Laborde, and Y. Renard (2008). "Mass redistribution method for finite element contact problems in elastodynamics". *European Journal of Mechanics, A/Solids* 27.5, pp. 918–932. DOI: 10.1016/j.euromechsol.2008.01.001. URL: https://hal.science/hal-00582045

Kiener, D. and S. M. Han (2022). "100 years after Griffith: From brittle bulk fracture to failure in 2D materials". *MRS Bulletin* 47.8, pp. 792–799. DOI: 10.1557/s43577-022-00379-2

Lasry, D. and T. Belytschko (1988). "Localization limiters in transient problems". *International Journal of Solids and Structures* 24.6, pp. 581–597. DOI: 10.1016/0020-7683(88)90059-5

Lebon, F. and R. Rizzoni (2022). "On the emergence of adhesion in asymptotic analysis of piecewise linear anisotropic elastic bonded joints". *European Journal of Mechanics - A/Solids* 93, p. 104512. DOI: 10.1016/j.euromechsol.2022.104512. URL: https://hal.science/hal-03546068

Meyer, C. and S. Walther (2022). "Optimal Control of Perfect Plasticity. Part I: Stress Tracking". *Mathematical control and related fields* 12.2, pp. 275–301. DOI: 10.3934/mcrf.2021022. URL: https://arxiv.org/abs/2001.02969

Moreau, J. J. (1978). "Approximation en graphe d'une évolution discontinue". fr. *RAIRO. Analyse numérique* 12.1, pp. 75–84. URL: https://hal.science/hal-01788586

Moreau, J. J. (1986). "Une formulation du contact à frottement sec ; application au calcul numérique". *Comptes Rendus de l'Academie des Sciences Serie II* 302.13, pp. 799–801. URL: https://hal.science/hal-01349850

Moreau, J. J. (1999). "Numerical aspects of the sweeping process". *Computer Methods in Applied Mechanics and Engineering* 177.3-4, pp. 329–349. DOI: 10.1016/s0045-7825(98)00387-9. URL: https://hal.science/hal-01349847

Moreau, J. J. (2004). "Indetermination due to dry friction in multibody dynamics". *European Congress on Computational Methods in Applied Sciences and Engineering*. ECCOMAS 2004 proceedings. Jyväskylä, Finland. URL: https://hal.science/hal-01825251

Moreau, J. J. (2006). "Facing the plurality of solutions in nonsmooth mechanics". *Nonsmooth/Nonconvex Mechanics with Applications in Engineering*. Ed. by C. C. Baniotopoulos. Thessalonique, Greece, pp. 3–12. URL: https://hal.science/hal-01824588

Moreau, J. J. (2011). "On Unilateral Constraints, Friction and Plasticity". *New Variational Techniques in Mathematical Physics*. Springer Berlin Heidelberg, pp. 171–322. DOI: 10.1007/978-3-642-10960-7_7

Needleman, A. (1988). "Material rate dependence and mesh sensitivity in localization problems". *Computer Methods in Applied Mechanics and Engineering* 67.1, pp. 69–85. DOI: 10.1016/0045-7825(88)90069-2

Niu, Z., V. Ziaei-Rad, Z. Wu, and Y. Shen (2022). "An asynchronous variational integrator for the phase field approach to dynamic fracture". *International Journal for Numerical Methods in Engineering* 124.2, pp. 434–457. DOI: 10.1002/nme.7127. URL: https://arxiv.org/abs/2203.08797

Pijaudier-Cabot, G. and Z. P. Bažant (1987). "Nonlocal damage theory". *Journal of Engineering Mechanics* 113.10, pp. 1512–1533. DOI: 10.1061/(ASCE)0733-9399(1987)113:10(1512)

Pinto Carvalho, R., A. M. Couto Carneiro, F. M. Andrade Pires, and A. Popp (2022). "An efficient algorithm for rigid/deformable contact interaction based on the dual mortar method". *Computational Mechanics* 71.1, pp. 143–167. DOI: 10.1007/s00466-022-02226-2. URL: https://arxiv.org/abs/2201.01165

Popp, A. and W. A. Wall (2014). "Dual mortar methods for computational contact mechanics – overview and recent developments". *GAMM-Mitteilungen* 37.1, pp. 66–84. DOI: 10.1002/gamm.201410004

Raffa, M. L., F. Lebon, and R. Rizzoni (2022). "A micromechanical model of a hard interface with micro-cracking damage". *International Journal of Mechanical Sciences* 216, p. 106974. DOI: 10.1016/j.ijmecsci.2021.106974. URL: https://hal.science/hal-03404654

Tkachuk, A., B. I. Wohlmuth, and M. Bischoff (2013). "Hybrid-mixed discretization of elasto-dynamic contact problems using consistent singular mass matrices". *International Journal for Numerical Methods in Engineering* 94.5, pp. 473–493. DOI: 10.1002/nme.4457

Wohlmuth, B. I. (2000). "A mortar finite element method using dual spaces for the Lagrange multiplier". *SIAM Journal on Numerical Analysis* 38.3, pp. 989–1012. DOI: 10.1137/s0036142999350929. URL: https://hal.science/hal-03747534

Wriggers, P. and T. A. Laursen (2007). *Computational Contact Mechanics*. Springer Vienna. DOI: 10.1007/978-3-211-77298-0

Zhang, X., Z. Qi, G. Wang, and S. Guo (2019). "Model smoothing method of contact-impact dynamics in flexible multibody systems". *Mechanism and Machine Theory* 138, pp. 124–148. DOI: 10.1016/j.mechmachtheory.2019.03.039